

# Significance of Inertance and Resistance in Fluidics of Thermal Ink-Jet Transducers\*

Narayan V. Deshpande

Wilson Center for Research and Technology, Xerox Corporation Webster, New York

## Abstract

The fluid flow in thermal ink-jet transducers is highly dynamic in the sense that at no time during its operation does the flow reach a steady-state condition. The transient flow is affected by the inertial and viscous effects. These two effects are reflected through the inertance and resistance parameters of the transducer geometry. In this study we present a general background on the inertance and resistance parameters, present a method for calculating these parameters for a given three-dimensional geometry, and briefly outline their role in the ink drop ejection process.

## Introduction

Thermal ink-jet (TIJ) is a drop-on-demand printing process. The printing element consists of a transducer and an ink-feeding system. The transducer is physically a miniature complex assembly that produces the ink drops in response to an electrical signal. The transducer has multiple channels, through which the ink flows, and each channel has a resistor that superheats the ink in contact with it when the electrical pulse is applied. The ink in contact with the resistor produces a vapor bubble that grows and pushes the ink out from the channel. After a short interval the vapor bubble collapses and an ink drop is ejected. Under the surface tension effect the channel is refilled and is ready to receive the next electrical pulse. The process is repeated for the next ink drop.

As a result of this periodic pulsing of the drop ejection process, the fluid flow through the channel is constantly changing as long as the printing process continues. Thus the flow through the ink passages is always transient. If the flow is stationary, the flow rate through a given passage, for a given pressure gradient, is governed by the viscous resistance of the passage. However, if the flow is transient, the flow rate is governed by not only the resistance, but also the inertance. The inertance results from the inertia of the fluid.

The fluid mechanics textbooks provide abundant information about the fluid resistance, but very little is discussed about the inertance. Furthermore, the fact that the resistance and inertance are functions of frequency is not elaborated. In this study we discuss these aspects and show how one can calculate these values for a given geometry. As an application we consider a channel geometry used in a TIJ printhead and show the significance of inertance and resistance in analyzing the flow characteristics of the printhead.

## Oscillating Flow through a Circular Pipe

To bring out the essential features of the transient flow, let us consider a simple problem of flow through a circular pipe subjected to a time-dependent pressure gradient. Assuming that the only nonzero velocity component is the axial velocity  $u = u(r,t)$ , the Navier–Stokes equation becomes

$$\rho \frac{\partial u}{\partial t} = -\frac{dp}{dx} + \mu \left( \frac{\partial^2 u}{\partial r^2} + \frac{1}{r} \frac{\partial u}{\partial r} \right), \quad (1)$$

where  $dp/dx$  is the pressure gradient,  $r$  is the radius, and  $\mu$  is the viscosity. If the pressure gradient varies sinusoidally with time, then we can assume

$$\frac{dp}{dx} = -G \exp(i\omega t). \quad (2)$$

It can be shown<sup>1</sup> that the solution for the velocity  $u$  is given by

$$u = \frac{G}{\rho} \exp(i\omega t) \left[ \frac{J_0 \left( \sqrt{\frac{-i\omega}{\nu}} r \right)}{J_0 \left( \sqrt{\frac{-i\omega}{\nu}} a \right)} \right], \quad (3)$$

where  $J_0$  is the Bessel function of the first kind,  $\nu$  is the kinematic viscosity,  $a$  is the radius of the pipe, and  $\omega$  is the frequency. The expression for flow rate  $q$  through the pipe can be obtained by integrating the velocity over the cross-sectional area of the pipe. The flow rate  $q$  is of the form

$$q = q_a \exp(i\omega t), \quad (4)$$

where  $q_a$  is the amplitude of the flow-rate. This is a complex number suggesting that the pressure and flow-rate fluctuations are out of phase with each other. The ratio of pressure gradient to flow rate is called the impedance,  $Z$ , which is also a complex number. We can express  $Z$  in the form

$$Z = R_\omega + i\omega L_\omega, \quad (5)$$

where  $R_\omega$  is the resistance and  $L_\omega$  is the inertance. The subscript  $\omega$  on the resistance and inertance indicates that they

both are functions of frequency  $\omega$ . Rezanka<sup>2</sup> has derived the full expression for  $Z$ .

### Lumped Parameter Model for Ink Flow Analysis

To study the refill process in a TIJ printhead, Torpey<sup>3</sup> derived an approximate lumped parameter equation in the form

$$L_\ell \frac{dq}{dt} + R_\ell q = \Delta p, \quad (6)$$

where  $L_\ell$  and  $R_\ell$  are the lumped element inductance and resistance, respectively, and  $\Delta p$  is the pressure difference across some length  $\ell$ . The lumped inductance and resistance for a circular pipe of radius  $a$  and length  $\ell$  are

$$L_\ell = \frac{\rho}{\pi} \left( \frac{\ell}{a^2} \right), \quad (7)$$

$$R_\ell = \frac{8\mu}{\pi} \left( \frac{\ell}{a^4} \right). \quad (8)$$

In view of the fact that the inductance and resistance are functions of frequency, the question arises as to how these lumped values relate to those defined in Eq. 5. Rezanka plotted the values of  $R/R_\ell$  and  $L/L_\ell$  as functions of frequency and made some interesting observations. He found out that the resistance equals the lumped element resistance at zero frequency, the resistance diverges as the square root of the frequency, the inductance equals the lumped element inductance at infinite frequency, and the limit of inductance at low frequencies is only 4/3 of its lumped element inductance. In mathematical terms the relation between lumped element values and exact values is given as

$$L_\ell = \lim_{\omega \rightarrow \infty} L_\omega, \quad (9)$$

$$R_\ell = \lim_{\omega \rightarrow 0} R_\omega. \quad (10)$$

We have used the case of a circular pipe to understand the relationship between the lumped element values and the exact values for the resistance and inductance. The relationship defined by Eqs. 9 and 10 is true in general. In our further discussion we consider only the lumped element values of the inductance and resistance, and for convenience we omit the subscript  $\ell$  on  $R$  and  $L$ . The question now is how can we determine the  $R$  and  $L$  values for any three-dimensional geometry. The answer is relatively simple. We calculate the flow rate  $q(t)$  as the response of the system to a step function in  $\Delta p$  and calculate the inductance and resistance from the following equations:

$$L = \frac{\Delta p}{\left( \frac{dq}{dt} \right)_{t=0}}, \quad (11)$$

$$R = \frac{\Delta p}{q(\infty)}. \quad (12)$$

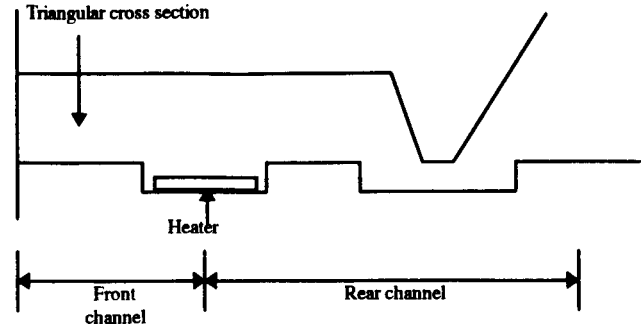


Figure 1. A channel geometry for a TIJ printhead.

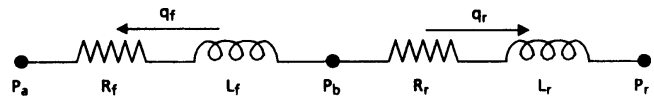


Figure 2. Lumped element model of the printhead.

The reason Eqs. 11 and 12 represent Eqs. 9 and 10, respectively, is that the step function excites all the frequencies; the system response at  $t = 0$  corresponds to the  $\omega \rightarrow \infty$  and the steady state corresponds to  $\omega \rightarrow 0$ . We will now consider a specific example to illustrate the case.

Figure 1 shows a channel geometry one might use for a TIJ printhead. The channel has a triangular cross section, and the heater is located in a recessed well as shown. The rear channel consists of a plug and a passageway around the plug for ink supply from the reservoir. This three-dimensional structure can be represented in a lumped element model as shown in Fig. 2. In Fig. 2,  $p_a$  is the ambient pressure,  $p_b$  the bubble pressure,  $p_r$  the reservoir pressure,  $L_f$  and  $R_f$  are the inductance and resistance of the front channel, and  $L_r$  and  $R_r$  are the corresponding values for the rear channel. The mid-position on the heater is used to divide the channel into front and rear sections.

The pressure in the bubble formed at the heater surface is very high at the instant of bubble formation, and it falls very rapidly as the bubble begins to expand.<sup>4,5</sup> The pressure becomes less than atmospheric within a few microseconds and remains at that level until the bubble collapses. For the lumped element model we can approximate the bubble pressure  $p_b$  as follows:

$$p_b(t) = \begin{cases} p_{\max} - (p_{\max} - p_{\min})(t/t_p) & \text{for } t \leq t_p \\ p_{\min} & \text{for } t \geq t_p, \end{cases} \quad (13)$$

where  $p_{\max}$  and  $p_{\min}$  are the maximum and minimum pressure values, and  $t_p$  is the time at which the pressure reaches  $p_{\min}$ . The impulse, i.e., the positive area under the pressure-time curve, rather than the exact value of  $p_{\max}$ , governs the flow behavior. For our example we have assumed  $p_{\max} = 30$  atm,  $p_{\min} = -0.6$  atm, and  $t_p = 1.4 \mu\text{s}$  with an approximate impulse of 21 atm-microseconds. For the pressure history assumed, the flow rate in the front channel section can be expressed as a solution of Eq. 6 as follows:

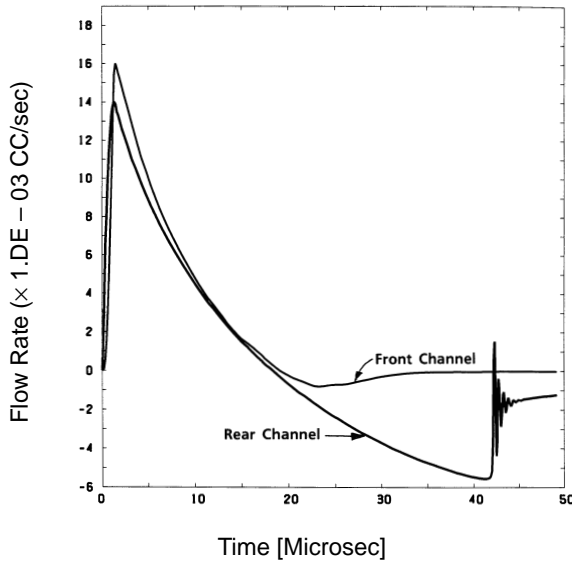


Figure 3. Flow rates in the front and rear channels of the transducer obtained from a full 3D calculation.

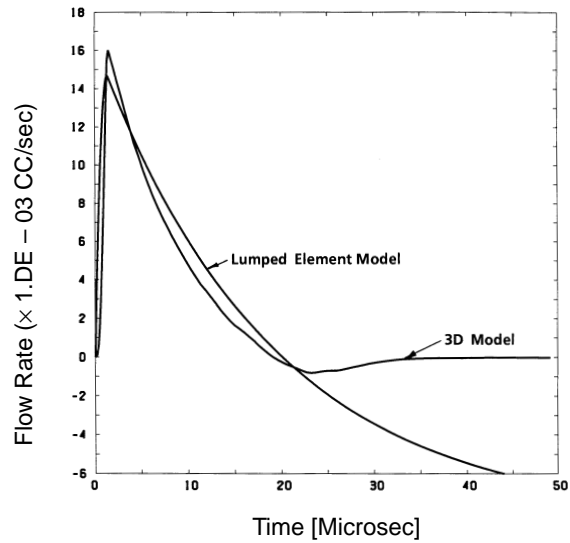


Figure 5. Comparison of flow rate in the front channel obtained from lumped element and 3D models.

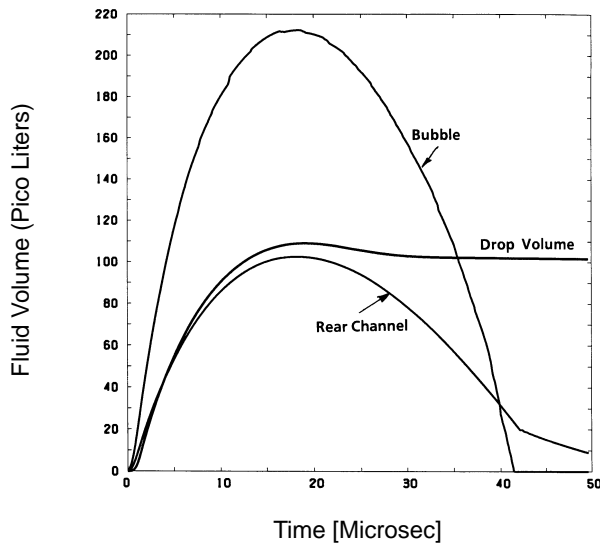


Figure 4. Volume of fluid displacement in the front and rear channel of the transducer and the bubble volume as a function of time calculated using a 3D model.

$$q_f(t) = \begin{cases} \frac{1}{R_f} \{ p_{\max} - p_a - (p_{\max} - p_{\min})(t - t_p) / t_p \} \\ - [p_{\max} - p_a + (p_{\max} - p_{\min})(t_f / t_p)] \\ \exp(-t / t_f) & \text{for } t \leq t_p \\ q_f(t_p) \exp((t_p - t) / t_f) + \frac{p_{\min} - p_a}{R_f} \\ [1 - \exp((t_p - t) / t_f)] & \text{for } t \geq t_p, \end{cases} \quad (14)$$

where  $q_f$  is the flow rate in the front channel of the transducer,  $R_f$  is the lumped element resistance of the front channel, and  $t_f = L_f / R_f$  is the characteristic time for the front chan-

nel. A similar expression can be obtained for the flow rate in the rear channel  $q_r$ , by replacing appropriate variables in Eq. 14.

### Comparison of the Lumped Element Model with Full 3D Model

We have used the CFD three-dimensional code FLOW-3D<sup>6</sup> to solve the flow in the three-dimensional geometry shown in Fig. 1 for the pressure history given in Eq. 13. The front and rear channel flow rates obtained for this case are shown in Fig. 3. The volume of fluid displaced in the front and rear channels and the bubble volume are shown in Fig. 4. Note that the bubble collapses at about 41  $\mu$ s after it is generated and the volume of the drop ejected is equal to 102 pL.

The same three-dimensional code is used to calculate the response of the front and rear channels to a stepped pressure input, and the resistances and inertances of the channels are calculated from Eqs. 11 and 12. For the particular set of dimensions used, these numbers come out to be  $R_f = 0.73747 \times 10^8$  g/(s, cm<sup>4</sup>),  $L_f = 1354.0$  g/cm<sup>4</sup>,  $R_r = 0.8440 \times 10^8$  g/(s, cm<sup>4</sup>), and  $L_r = 1619.0$  g/cm<sup>4</sup>. These values are substituted in Eq. 14 to obtain the lumped parameter solution. Figure 5 shows the comparison of flow rate in the front channel between the lumped element model and the full three-dimensional model. The agreement is very good until the time the fluid meniscus begins to retract into the front channel. This occurs at about 25  $\mu$ s and then the drop breakoff occurs at about 30  $\mu$ s. The retraction of the meniscus into the channel modifies the inertance and resistance values, and the two solutions deviate after that point.

By integrating the flow rate we can calculate the volume displacement as a function of time. The results are shown in Fig. 6 for the lumped and three-dimensional cases. The peak values are 128 pL and 108 pL for the two cases, respectively. The drop volume from three-dimensional calculations is 102 pL. Thus if we use the peak value as an approximate measure of the drop volume, the error in using the lumped model re-

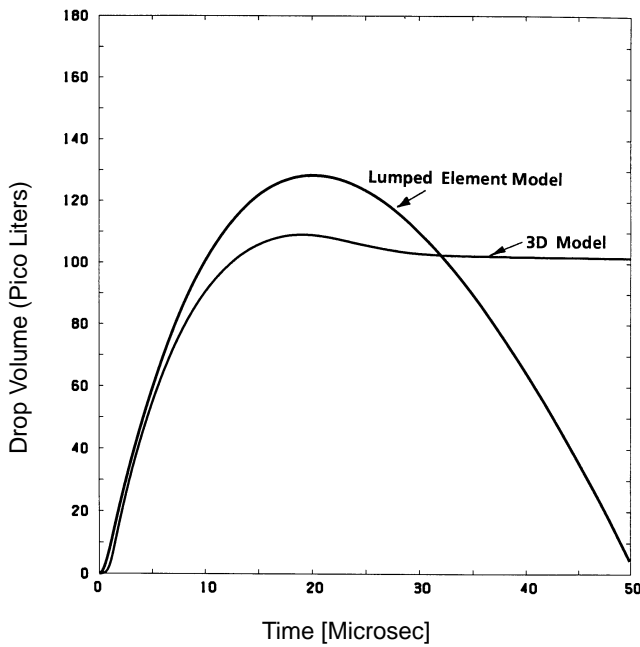


Figure 6. Comparison of front channel fluid volume displacement in the lumped element and 3D models.

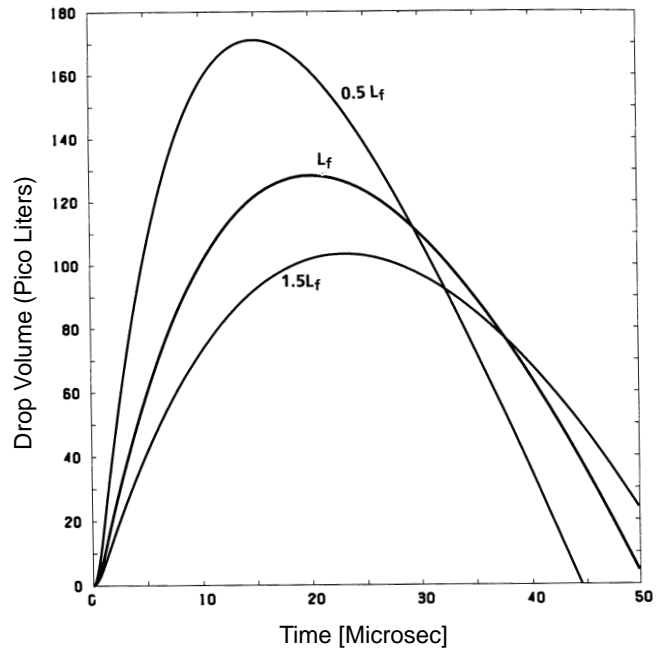


Figure 8. Fluid volume displacement in the front channel for three values of inertia.

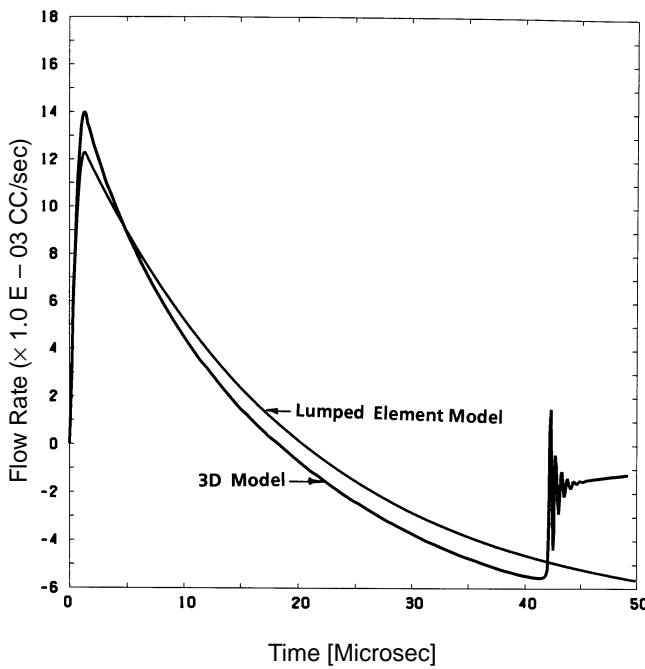


Figure 7. Flow rate in the rear channel obtained from the lumped element and 3D models.

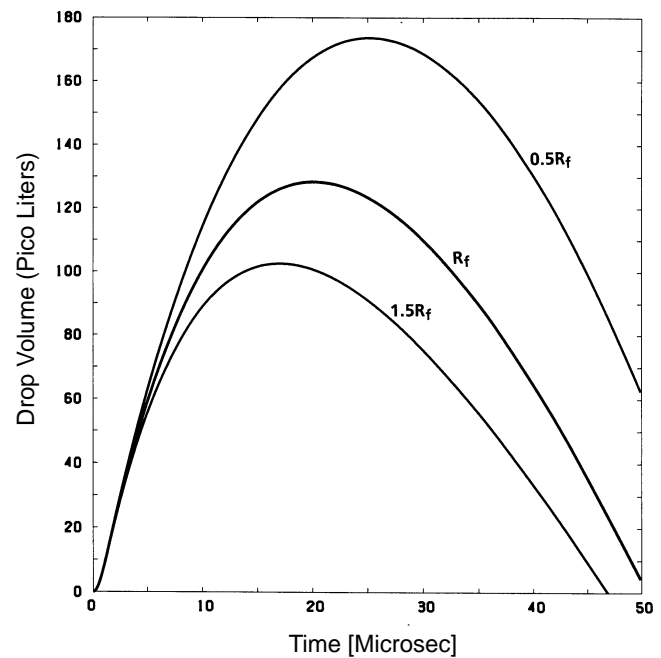


Figure 9. Fluid volume displacement in the front channel for three values of resistance.

sults is less than 20%. The three-dimensional model calculations require a few hours of CPU on a Sparc workstation, whereas the lump element model calculations take only a few milliseconds. Thus one can get a very good and fast estimate of the performance of a given structure of a TIJ transducer using the lumped element model. One may estimate the inertia and resistance values for the given structure by calculating an equivalent radius and using Eqs. 7 and 8.

In a similar manner we can calculate the flow in the rear channel. Figure 7 shows the comparison of flow rates in the rear channel obtained from the lumped element model and the three-dimensional model. It again shows very good agreement until the bubble collapse time. At the bubble collapse time there is a very high pressure impulse for a very short duration. The flow is abruptly brought to rest and some ringing occurs, as seen in the figure. The volume displacement

can be calculated in this case also and additional information can be obtained about the flow, but it is not discussed here.

### Effect of Inertance and Resistance Change

We can use the lumped element model of the channel geometry to understand the effect of changing the geometry. When the geometry changes, both the inertance and resistance will change, but for illustrative purposes we can change these numbers independently and study their effects. We will consider only the front channel geometry and calculate the drop volume estimate. Figure 8 shows the effect of changing the inertance. It shows that increasing the inertance decreases the drop volume. The initial slope of the volume curve is an indication of the drop velocity. The results show that the drop velocity will also decrease with increasing inertance.

Figure 9 shows the effect of changing the resistance of the front channel. In this case also, an increase in the resistance decreases the drop volume, but the drop velocity seems to be unchanged. The peaks in these curves occur at different times and the retraction of the meniscus is also probably significantly different for these cases, and one can make additional inferences on the behavior of the channel geometry.

### Summary

A brief outline of the origin of the inertance and resistance for a fluidic system is given and the dependence of these properties on the frequency of excitation is brought out. The connection between frequency-dependent values and the lumped element representation values is pointed out and a method to calculate these values for any three-dimensional geometry is

outlined. As an example, a geometry used for a TIJ transducer is considered, and the inertance and resistance of that geometry is calculated. A lumped element model of the transducer is used to obtain the flow through the transducer during the drop ejection process, and it is shown that the results are in close agreement with those obtained with a full three-dimensional CFD code. The lumped element model is used to investigate the effects of resistance and inertance change on the performance of the transducer, and it is shown that both the inertance and the resistance of the front section of the channel govern the drop volume and drop velocity from the transducer.

### References

1. F. M. White, *Viscous Fluid Flow*, McGraw-Hill, New York, 1974, p. 143.
2. I. Rezanka, Impedance of viscous fluid in a circular pipe, Xerox Internal Report X9200581, December 1992.
3. P. A. Torpey, Effect of refill dynamics on frequency response and print quality in a drop-on-demand ink jet system, *Proceedings SPSE's Third International Congress on Advances in Non-Impact Printing Technologies*, p. 89 (1986).
4. P. A. Torpey, Prevention of air ingestion in a thermal ink jet device, *Proceedings SPSE's Fourth International Congress on Advances in Non-Impact Printing Technologies*, p. 275 (1988).
5. N. V. Deshpande, Fluid mechanics of bubble growth and collapse in a thermal ink jet printhead, *Proceedings SPIE—Hard Copy Output*, p. 273 (1989).
6. FLOW—3D Computational Modeling Power for Scientist and Engineers, Flow Science, Los Alamos, NM.